DUNSTON ANGELINE KIRUBA (ORCID: 0000-0002-9241-1143)[1]
KARPAGASUNDARAM MUTHUKUMARAN (ORCID: 0000-0002-5743-7559)[2]
PERUMAL THAMARAI (ORCID: 0000-0003-4660-1787)[3]

REMOVAL OF Ni(II) IONS FROM AQUEOUS SOLUTIONS USING MANGANESE OXIDE NANOPARTICLES FROM BUFFELGRASS, *CENCHRUS CILIARIS* L., AS GREEN ADSORBENT. KINETICS AND THERMODYNAMICS STUDIES

Manganese oxide nanoparticles (MnONPs) synthesized from buffelgrass, *Cenchrus ciliaris* (L.), an invasive weed posing threats to ecosystems, are used in this study to remove nickel(II) ions from aqueous solutions. As a biosorbent, the synthesized MnONPs were put to the test. MnONPs were studied for their surface morphology and functional properties. A variety of adsorbent dosages and contact times were tested in batch experiments to see how they affected adsorption rates. At pH 6.0 and room temperature, MnONPs had an 87.1% removal efficiency for Ni(II) ions. Pseudo-second order correlations had a higher R^2 value (0.988). In the Langmuir plot, a maximum adsorption capacity of 4.78 mg/g was observed. However, the experimental data fitted well with both Langmuir and Freundlich isotherm models ($R^2 = 0.99$). Spontaneous and exothermic was the nature of the adsorption process. To remove heavy metal ions contaminants from aqueous solutions, these results suggested that MnONPs synthesized from buffelgrass extract could be used.

1. INTRODUCTION

Pollution from heavy metal ions is one of the most significant environmental issues today, posing a serious risk to people's health all over the world. Tremendous growth and development of industries have led to a spike in the heavy metal ions release into

_____

[1]Department of Industrial Biotechnology, Government College of Technology, Coimbatore, Tamilnadu, India, Pincode-641013, corresponding author, email address: angeline87gct@gmail.com
[2]Hindusthan College of Engineering and Technology, Coimbatore, Tamilnadu, India, Pincode-641032.
[3]Government College of Technology, Coimbatore, Tamilnadu, India, Pincode-641013.

the environment. Heavy metal ions enter the food chain resulting in their bio-accumulation, causing varied adverse effects on human health as well as aquatic living things because of their toxicity and carcinogenicity. The persistence of such hazardous heavy metal ions contaminants is of great public concern since they are not biodegradable. The most common heavy metal ion contaminants found in industrial effluents are lead(II), cadmium(II), copper(II), cadmium(II), zinc(II), and nickel(II). Nickel is routinely used for commercial purposes in automobile industries, plating industries, electronics as catalysts, household products, and cheap jewelry [1]. According to the Bureau of Indian Standards, 2012, the permissible limit of Ni(II) ions for drinking water is 0.02 mg/dm^3. As per the Indian Environment Protection Rules 1986, the permissible limit for inland surface water, public sewers, and common effluent treatment plants is 3.0 mg/dm^3. Heavy metal ions, including nickel(II), were found to be present in high concentrations in water taken from wetlands in Coimbatore, southern India, according to a previous study [2]. Moreover, the prevalence of cancers has become evident among nickel alloy welders, nickel catalyst operators, nickel electrolysis workers, and foundrymen [3].

Hence, efficient technology has to be adapted to remove nickel(II) ions before they get accumulated in water reserves, threatening the ecosystem. Adsorption is one of the most cost-effective, flexible, and high-quality water treatment methods available [4]. The expected high surface area and improved reactive sites of nanostructured particles of biotic origin have made them important in this category despite the widespread use of low-cost adsorbents for wastewater treatment. Nanosized manganese oxide particles having polymorphic structures and high specific surface area exhibit remarkable performance in various applications including catalysis, water treatment, as image contrasting agents, biosensors, and energy storage materials [5]. Manganese oxide prepared in various forms has been employed in diverse fields as given in Table 1.

Table 1. Applications of manganese oxides in various fields

Forms of manganese oxide	Environmental/industrial applications
Manganese oxide-coated carbon nanotubes	removal of lead(II) from aqueous solution [7]
Manganese oxide coated zeolite	removal of copper(II) and lead(II) ions from solution [8]
Pyrolusite, a manganese ore consisting mainly MnO$_2$	copper(II) adsorption [9]
Manganese oxide-modified biochars	removal of arsenic(V) and lead(II) [10]
Manganese-oxide-coated alumina	defluoridation [11]
Bimetal adsorbent of Mn-oxide-doped Al oxide	arsenic(III) adsorption [12]
Manganese oxide/graphene oxide composite Manganese oxide nanorods supported onto orange peel-based carbon	electrochemical capacitors [13,14]
Green synthesized manganese nanoparticles	antimicrobial agents [15]

Although various chemical and biogenic methods are routinely adapted for the synthesis of nanoparticles, it is imperative to explore a green synthesis route that could be

a cost-effective technique for the synthesis of nanoparticles and plants used in the reduction of potassium permanganate for the synthesis of manganese oxide nanoparticles (MnONPs) would be easily available. Nanoparticles made with the leaf extract of buffelgrass (Poaceae) (*Cenchrus ciliaris* L.) were used in this study to remove nickel ions. Buffelgrass, one of the most common forage plants in South Asia, is now being reported as an invasive species, taking over native habitats [6]. Nickel(II) ions in the industrial effluents are not biodegradable and their existence in receiving lakes and streams leads to severe health-related problems in plants, aquatic organisms, animals including human beings. Hence, an attempt was made (1) to synthesize MnONPs using the leaves extract of buffelgrass; (2) to characterize the synthesized MnONPs using Raman spectroscopy, FTIR, XRD, and HRTEM/SEM-EDS; (3) to evaluate adsorptive efficiency of MnONPs in the removal of Ni(II) ions from aqueous solutions, and (4) to study the dynamics, isotherms, and thermodynamics of adsorption.

2. EXPERIMENTAL

Materials. The precursor used in the synthesis of MnONPs, potassium permanganate (analytical grade), nickel(II) sulfate hexahydrate used as adsorbate, and sodium hydroxide employed as a desorbing agent were procured from HiMedia Pvt., Ltd., India.

Sample preparation. Fresh leaves of *Cenchrus ciliaris* L. (25 g) were washed twice with double distilled water and grounded in 100 cm^3 of distilled water using mortar and pestle and allowed to settle down for 30 min. The supernatant was filtered and the filtrate was constantly stirred for 1 h using a magnetic stirrer.

Synthesis of manganese oxide nanoparticles. The leaf extract of *Cenchrus ciliaris* L. and $KMnO_4$ (1 mol/dm^3) were mixed in the ratio of 15:85 for a total volume of 100 cm^3. The mixture was kept at room temperature for 2–3 days to enhance the production of manganese oxide nanoparticles. The disappearance of the purple color of potassium permanganate and the appearance of brown-colored precipitates indicated the formation of manganese oxide nanoparticles. The reaction mixture was then centrifuged for 10 min at 2500 rpm to remove the nanoparticles. To facilitate annealing, the slurry was kept at 100 °C in a hot air oven and then subjected to 400 °C for 2 h to produce nanoparticles in a powder form. The phyto-reductants of *Cenchrus ciliaris* L. are involved in the redox process and subsequent stabilization of nanosized manganese oxide particles. The particles were subjected to UV-visible spectrophotometric analysis (Systronics) in the wavelength range of 200–800 nm. The appearance of the absorption edge at 360 nm is a clear indication of the formation of manganese oxide nanoparticles.

Characterization of MnONPs. MnONPs were subjected to Raman spectroscopy to observe vibrational, rotational, and other low-frequency modes. The reactivity and properties of any material are influenced by the presence of various functional groups and

the type of coating material. Green synthesized MnONPs were identified using Fourier transform infrared spectroscopy (FT-IR) (Perkin Elmer) in the range 4000–450 cm^{-1}. Background correction was done using pure KBr and an FTIR spectrum was recorded. SEM (Zeiss) images of the MnONPs were taken to better understand their morphology. Energy-dispersive X-ray spectroscopic analysis (EDX) was used to analyze the elements present in MnONPs. High resolution transmission electron microscopy (HRTEM) and selected area electron diffraction (SAED) image analysis (JEOL JEM 2100 operated at an accelerating voltage of 200 kV) were used to determine their particle size and morphology. The sample suspension was kept on a carbon-coated copper grid and evaporated in a vacuum desiccator for 20 min. Analysis of the crystallinity of MnONPs using a powder XRD (Bruker D8 Advance Powder X-ray Diffractometer, Germany), with Cu-Kα radiation ($\lambda = 1.54060$ Å) was performed. Diffractograms were recorded at room temperature in the range of 2θ angle from 20° to 90° with the scanning speed of two degrees per minute. The particles were calcined at 400 °C before PXRD analysis to remove moisture content.

Batch adsorption experiments using manganese oxide nanoparticles. Manganese oxide nanoparticles synthesized from grass leaf extract were used as an adsorbent for the removal of Ni(II) ions from an aqueous environment. In terms of contact time (0–120 min), pH (2.0–8.0), and doses of 0.2-1 g/dm^3, adsorption capacity and percentage removal were investigated. The initial concentration of Ni(II) was retained at 10 mg/dm^3 for adsorption optimization studies. Concentrations in the range of 1–10 mg/dm^3 mimicked the low-concentration contamination conditions commonly found in treated industrial effluent. All of these tests used Atomic Absorption Spectroscopy (AAS) (Agilent) to estimate the remaining concentration of metal ions in the aliquot. Isotherm and kinetic models were used to analyze adsorption data obtained from this experiment. The influence of temperature on the adsorption process was studied by varying temperatures from 303 to 333 K.

Isotherm studies. The adsorption behavior was investigated using the Langmuir isotherm and Freundlich isotherm models.

The linearized Langmuir isotherm is represented by

$$\frac{C_e}{q_e} = \frac{1}{Q_m b_L} + \frac{C_e}{Q_m}$$

(1)

where q_e is the amount of metal ion adsorbed at equilibrium, mg/g, C_e is the equilibrium concentration of the adsorbate, mg/dm^3, Q_m, mg/g, and b_L, dm^3/mg, are the Langmuir constants related to adsorption capacity and energy of adsorption, respectively.

Separation parameter values (R_L) which reveal the nature of the adsorption process is given by

$$R_L = \frac{1}{1 + b_L C_0} \tag{2}$$

where C_0 is the initial metal ion concentration, mg/dm^3.

The Freundlich equation for sorption on a heterogeneous surface can be expressed as

$$\ln q_e = \ln K_F + \frac{1}{n} \ln C_e \tag{3}$$

where K_F, mg/g, is the Freundlich constant and n is the Freundlich exponent.

The Langmuir and Freundlich adsorption isotherms were studied using the established liquid isotherm equations from the experiments.

Kinetics studies. Pseudo-first- and pseudo-second order kinetic models were examined in this research. The following equation can be used to explain the pseudo-first order rate expression [16] based on solid capacity

$$\frac{dq_t}{dt} = k_1 (q_e - q_t) \tag{4}$$

The linearized form of pseudo-first order rate expression is given as:

$$\log(q_e - q_t) = \log q_e - \frac{k_1 t}{2.303} \tag{5}$$

where q_e is the amount of metal ions adsorbed at equilibrium, mg/g, q_t is the amount adsorbed at time t, mg/g, k_1 is the pseudo-first order rate constant, min^{-1}. The straight-line plot of $\log(q_e - q_t)$ against time was used to calculate the value of the adsorption rate constant k_1 for the adsorption.

It is given by the following equation that the pseudo-second order kinetics [17] exists:

$$\frac{dq_t}{dt} = k_2 (q_e - q_t)^2 \tag{6}$$

The linearized form of equation (6) after integration is given as:

$$\frac{t}{q_t} = \frac{1}{k_2 q_e^2} + \frac{t}{q_e} \tag{7}$$

where k_2 is the pseudo-second order rate constant, g/(mg·min). The value of k_2 was determined from the plot of t/q_t against t.

Thermodynamics studies of Ni(II) adsorption on MnONPs. Adsorption experiments were conducted at 303, 313, 323 and 333 K. Gibbs free energy, $\Delta G°$, kJ/mol,

enthalpy, $\Delta H°$, kJ/mol, and entropy $\Delta S°$, kJ/(mol·K), were calculated as expressed in equations

$$\Delta G° = -RT \ln K_c \tag{8}$$

where R is the molar gas constant (8.314 J/(K·mol)), T is the absolute temperature, K, Equilibrium constant K_C is the distribution ratio of equilibrium concentrations of adsorbate in the adsorbed state (C_{ad}) to equilibrium concentrations of adsorbate present in the solution (C_e)

$$K_C = \frac{C_{ad}}{C_e} \tag{9}$$

$$\ln K_C = -\frac{\Delta H°}{RT} + \frac{\Delta S°}{R} \tag{10}$$

Enthalpy and entropy changes were calculated from the slope ($-\Delta H°/R$) and the intercept ($\Delta S°/R$) of the plot $\ln K_C$ against $1/T$, respectively.

3. RESULTS AND DISCUSSION

3.1. CHARACTERIZATION OF MnONPs

Raman spectrum (not presented here) with bands between 500 and 700 cm^{-1} corresponding to the characteristic stretching vibrations of O–Mn–O demonstrated the presence of the MnO$_2$ in the sample which is following the earlier reports [18]. The potential of nanoparticles depends upon the chemical reactivity and the properties of the functional groups and their contribution to surface chemistry.
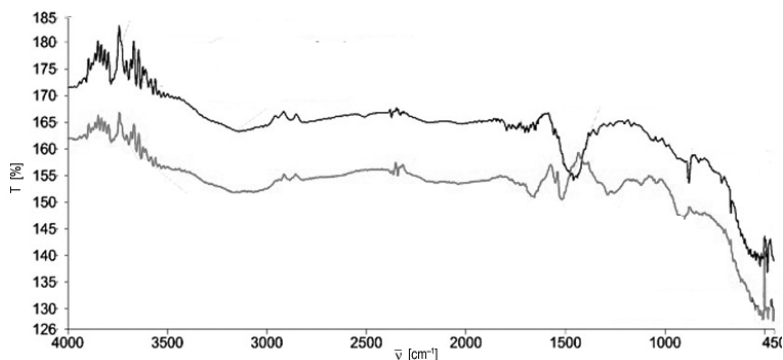
Fig. 1. FT-IR spectrum of MnONPs before and after adsorption

The functional groups of MnONPs before and after adsorption of heavy metal ions were verified using Fourier transform infrared spectroscopy (FT-IR) (Fig. 1) representing the shift in the wavenumber of dominant peaks associated with the spectrum of MnONPs. The spectrum of MnONPs before adsorption shows the presence of intense peaks between 505 and 480 cm^{-1} attributing to the stretching vibration of Mn–O bond; the peak at 1654 cm^{-1} denotes C=O stretching; the peak at 1518 cm^{-1} denotes N–H bending mode and the peak at 3696 cm^{-1} might be due to the –OH stretching of water or ethanol [19]. Similar peaks were observed in MnONPs after adsorption but at different wavelengths because of the interaction of metal ions with the synthesized MnONPs.
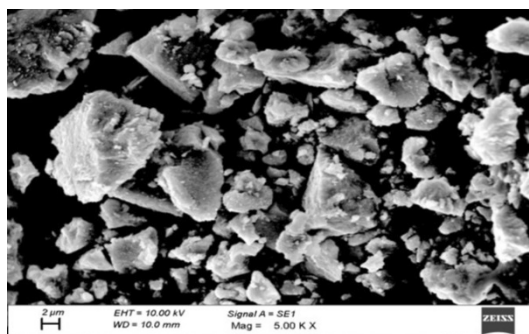
Fig. 2. SEM micrograph of MnONPs
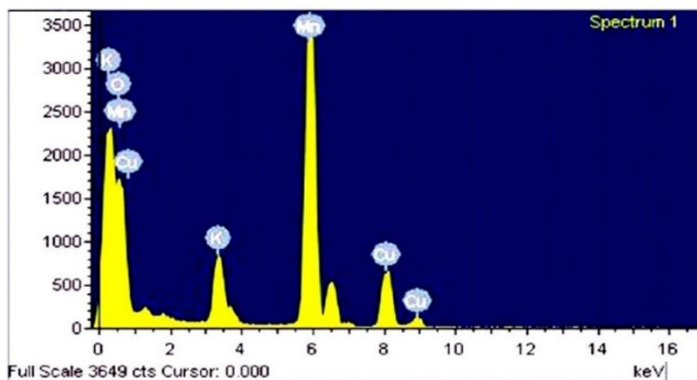
Fig. 3. EDX spectrum of MnONPs

SEM (Fig. 2) and EDX spectrum (Fig. 3) of MnONPs revealed the morphology and the elemental composition of the analyte, respectively. HRTEM micrographs (Fig. 4a) of MnONPs revealed the formation of hexagonal shaped nanoparticles of weak crystalline nature leading to a certain degree of aggregation. Figure 4b shows the diffraction rings of SAED pattern which were found to be distinct and have reduced due to agglomeration of the particles. The X-ray diffraction pattern of MnONPs is presented in Fig. 5.
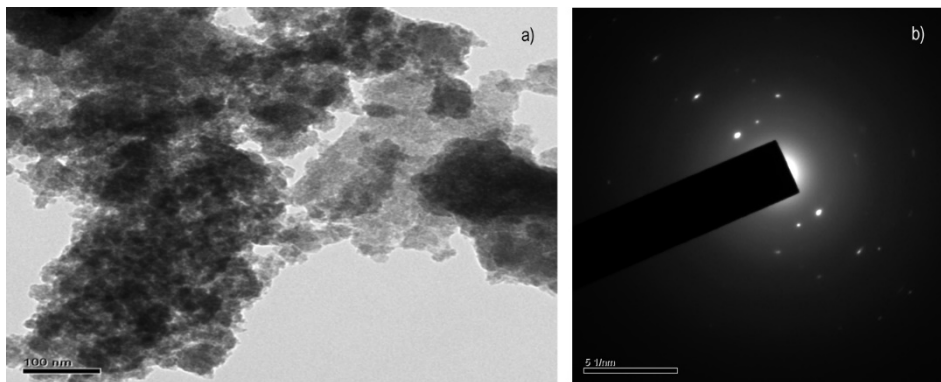
Fig. 4. HRTEM micrograph of MnONPs (a), and SAED pattern of MnONPs (b)
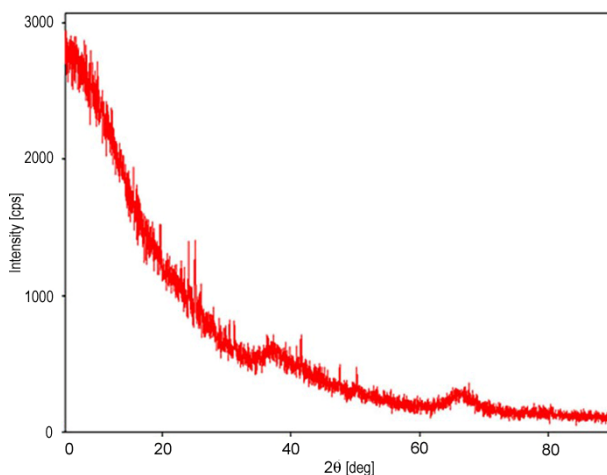
Fig. 5. PXRD pattern of MnONPs

Two distinct peaks at 2θ angles, 37° and 65° which are representative of the birnessite phase of MnO_2 corresponding to the crystalline planes (311) and (440) were observed [20]. This observation was following JCPDS-42-1169 of manganese oxide nanoparticles [14]. The full width at half maximum (FWHM) values measured from PXRD patterns was substituted in Debye–Scherrer's equation and the particle size was measured as 70 nm.

3.2. EVALUATION OF ADSORPTION EFFICIENCY

The adsorption experiments were carried out at various contact times ranging from 20 to 120 min with Ni(II) ions concentration of 10 mg/dm^3, 0.2 g/dm^3 of MnO_2 nanoparticles, and pH of 6.0. The adsorption efficiency gradually increased upon time, then

reached a plateau where maximum removal was observed, i.e., 80 min (Fig. 6). Fe$_3$O$_4$ impregnated tea waste as an adsorbent for the removal of Ni(II) ions showed a similar pattern [21].
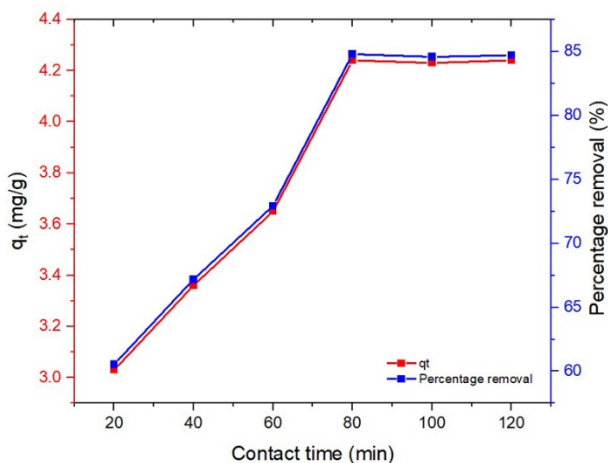
Fig. 6. Effect of contact time on Ni(II) removal efficiency and adsorption capacity; initial Ni(II) ion concentration 10 mg/dm^3, adsorbent dose 0.2 g/dm^3, pH 6
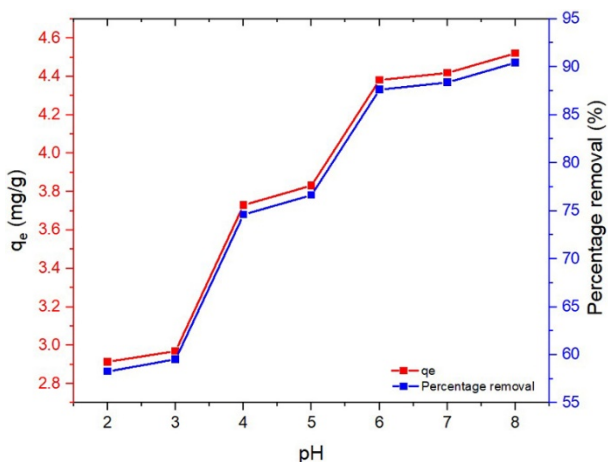
Fig. 7. Effect of pH on Ni(II) removal efficiency and adsorption capacity; initial Ni(II) ion concentration 10 mg/dm^3, adsorbent dose 0.2 g/dm^3, contact time 80 min

Solubility, adsorption capacity, and counter-ion adsorption are all affected by the pH of a solution, which is one of the most important factors in the process. To investigate the impact of pH, the initial pH of the solution was varied from 2 to 8. The high concentration of H$^+$ ions in the acidic environment could explain the low adsorption

efficiency at lower pH. The competition between H^+ ions and Ni(II) ions decreased as the pH is increased, allowing the metal ions to get adsorbed more easily. pH 6 was found to be the optimum pH for the removal of Ni(II) ions; after that, the removal percentage increased, possibly as a result of the formation of hydroxyl metal precipitates at higher pHs (Fig. 7).
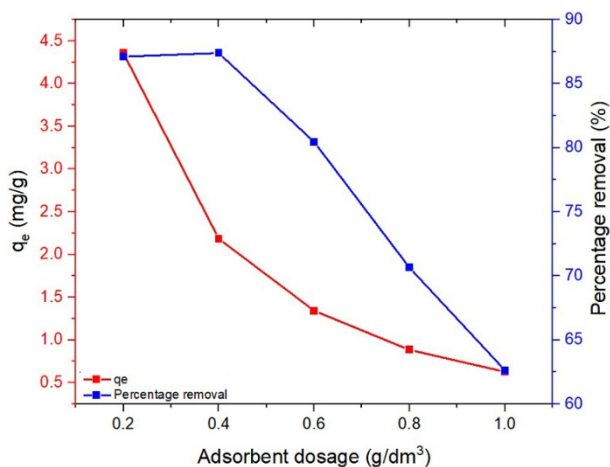
Fig. 8. Effect of adsorbent dosage on Ni(II) removal efficiency and adsorption capacity; initial Ni(II) ion concentration 10 mg/dm³, contact time 80 min, pH 6

The adsorbent dosage has a significant impact on the adsorption capacity. When the number of adsorption sites available to the adsorbate is increased, better adsorption occurs. As shown in Fig. 8, the removal percentage increased only from 87.1 to 87.38% when the dosage was increased from 0.2 to 0.4 g/dm³, and then it decreased as the dosage is increased up to the maximum of 1 g/dm³. This could be due to the overlapping of adsorption sites as reported earlier in the adsorption of fluoride using processed biochar [22]. In addition, a decrease in adsorption capacity was observed with increasing adsorbent dosage, since adsorption capacity and adsorption dosage are inversely proportional to each other. Manganese oxide nanoparticle dose of 0.2 g/dm³ at an optimum pH of 6 resulted in the removal percentage of 87.1% of Ni(II) ions. The adsorption process could be further optimized at varying temperatures since the change in pH may affect the process conditions.

3.3. ISOTHERM STUDIES

The Langmuir isotherm assumes an independent amount of adsorbed enthalpy while the Freundlich equation assumes that the adsorption enthalpy on a heterogeneous surface decreases logarithmically upon increasing fraction of adsorbed sites. Using R^2 and other isotherm parameters, the metal ion adsorption data was fitted to the Langmuir

isotherm model (Fig. 9). The results are shown in Table 2. R^2 values show that the experimental data fitted well with the Langmuir isotherm model. Nickel(II) adsorption onto manganese oxide nanoparticles was found to be favorable, with R_L values of 0–1. The maximum adsorption capacity was 4.78 mg/g. According to the electronegativity of the metals and the cation/anion state of the ions, the adsorption capacity could be explained [23]. Earlier studies showed that the adsorption capacity for the removal of Ni(II) ions was 0.001, 0.03, 1.1, and 1.5 mg/g for bagasse, fly ash, *Aspergillus niger*, and granular activated carbon, respectively [21]. In this study, the green synthesized metal oxide nanoparticles used for the removal of Ni(II) ions showed reasonable adsorption capacity, and the supremacy of the synthesized nanoparticles is proven by their non-toxic and eco-friendly nature.
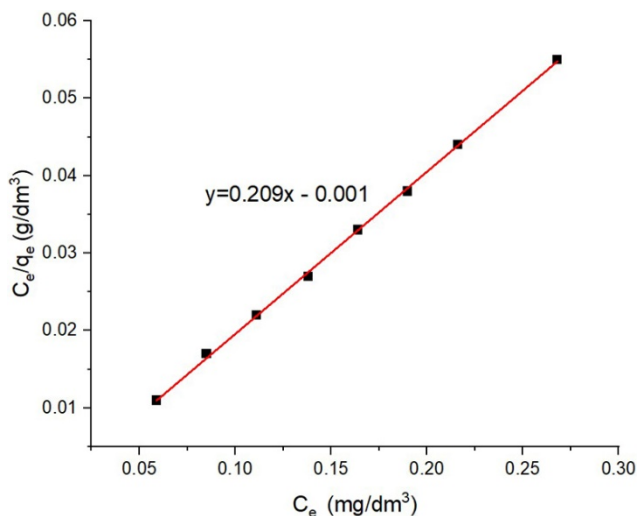
Fig. 9. Langmuir isotherm (linearized) for MnONPs

T a b l e 2

Isotherm parameters for the adsorption of Ni(II) ions onto MnONPs

Langmuir isotherm			Freundlich isotherm		
R^2	Q_m [mg/g]	b_L [dm³/mg]	R^2	K_F [mg/g]	n
0.999	4.78	0.004	0.999	4.94	10

Table 2 lists the values of Freundlich isotherm constants as well as the corresponding correlation coefficients. Since the *n* value was between 1 and 10, and K_F was greater than 1, the adsorption was found to be good and the adsorption capacity was significant (Fig. 10).
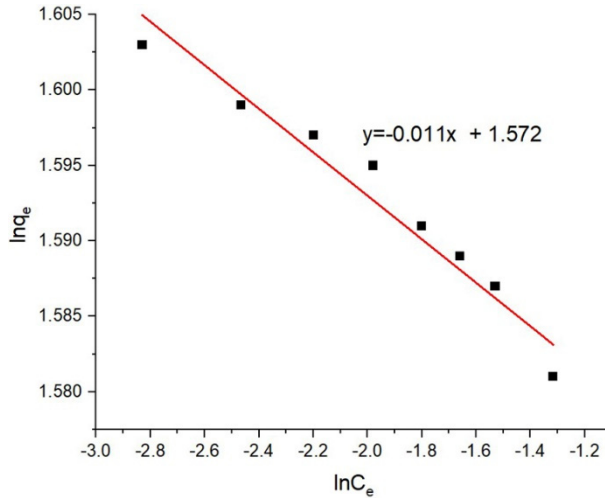
Fig. 10. Freundlich isotherm (linearized) for MnONPs

3.4. ADSORPTION KINETICS AND THERMODYNAMICS STUDIES

Adsorbate-solid phase adsorbent dynamic interactions were studied to identify possible rate-controlling steps and the adsorbate-solid-phase adsorbent dynamic interactions over time [24]. Based on the plot of $\log(q_e - q_t)$ and time the pseudo-first order constant k_1 and the correlation coefficient R^2 were found to be –0.026 min^{-1} and 0.82, respectively. As predicted by the pseudo-first order kinetic models, adsorption capacities ($q_{e\text{cal}}$) did not agree with experimental capacities ($q_{e\text{exp}}$). The values for the adsorption rate constant (k_1) obtained using the model were found to be negative.

From the dependence of t/q_t on time, pseudo-second order kinetics is depicted by the straight line with a slope of $1/q_e$ and an intercept of $1/k_2 q_e^2$, which gives the values of the two key parameters (k_2 and q_e) as 0.0065 min^{-1} and 3.84 mg/g, respectively (Table 3). For the adsorption of nickel(II) ions, the pseudo-second-order kinetics model fits fairly well with the experimental data.

T a b l e 3

Kinetics parameters for the adsorption of Ni(II) ions onto MnONPs

Pseudo-first-order kinetics				Pseudo-second order kinetics			
R^2	k_1 [min^{-1}]	$q_{e\text{exp}}$ [mg/g]	$q_{e\text{cal}}$ [mg/g]	R^2	k_2 [g/(mg·min)]	$q_{e\text{exp}}$ [mg/g]	$q_{e\text{cal}}$ [mg/g]
0.820	–0.026	2.568	6.5	0.988	0.0065	2.568	3.84

Analysis of thermodynamics was done and the parameters, such as the free energy change ($\Delta G°$), enthalpy ($\Delta H°$), and entropy ($\Delta S°$) were calculated as shown in Table 4

at various temperatures. Linearity was found in the plot of $\ln(K_c)$ against $1/T$, with correlation coefficients, R^2 of 0.995, and $\Delta H°$ and $\Delta S°$ were calculated from the slope and intercept of the plot.

Table 4

Thermodynamic parameters for the adsorption of Ni(II) ions onto MnONPs

Temperature [K]	$\Delta G°$ [kJ/mol]	$\Delta H°$ [kJ/mol]	$\Delta S°$ [kJ/(mol·K)]	R^2
303	−2.7			
313	−1.3	−47	−146	0.995
323	−0.08			
333	0.6			

Ni(II) ion adsorption is exothermic since $\Delta S°$ and $\Delta H°$ are negative. The increase in temperature did not affect the adsorption process, indicating that it is physisorptive in nature [25]. The negative $\Delta G°$ values at 303, 313, and 323 K, and $\Delta G°$ value closer to 0 at 333 K showed that the adsorption process was both spontaneous and thermodynamically favorable. In general, adsorption processes with $\Delta G°$ values of –20 kJ/mol to 0 indicate that the process is spontaneous [26].

4. CONCLUSION

The green synthesis of MnONPs using the leaf extract of buffelgrass, *Cenchrus ciliaris* L., was demonstrated in this study, a cost-effective method that does not require expensive equipment and reaction catalysts. MnONPs have been thoroughly characterized in terms of their optical, morphological, and functional attributes. Ni(II) ion removal using MnONPs was found to be affected by pH, adsorbent dosage, and contact time. The adsorption capacity was measured as 4.78 mg/g. The experimental data fitted well with the pseudo-second order kinetics model and the equilibrium data fitted well with both Langmuir and Freundlich isotherm models. The exothermic, spontaneous nature, and physisorption behavior of the process was ascertained from the thermodynamic analysis. This study may be useful for wastewater treatment for the removal of Ni(II) ions. This research can be expanded to check the feasibility for the removal of other heavy metal ions and contaminants that causes ecotoxicity and environmental pollution.

REFERENCES

[1] GENCHI G., CAROCCI A., LAURIA G., SINICROPI M.S, CATALANO A., *Nickel: human health and environmental toxicology*, Int. J. Environ. Res. Public Health, 2020, 17 (679), 1–21. DOI: 10.3390 /ijerph17030679.

[2] PAVITHRAPRIYA S., MAHIMAIRAJA S., KARUPPUSAMY S., *Pollution due to heavy metals in Coimbatore Wetlands, India*, Res. J. Agr. Forest. Sci., 2015, 3 (6), 1–5.

[3] SAVOLAINEN H., *Biochemical and clinical aspects of nickel toxicity*, Rev. Environ. Health, 1996, 11 (4), 167–173. DOI: 10.1515/reveh.1996.11.4.167.

[4] GONG J.L., WANG X.Y., ZENG G.M., CHEN L., DENG J.H., ZHANG X.R., NIU Q.Y., *Copper(II) removal by pectin iron oxide magnetic nanocomposite adsorbent*, Chem. Eng., 2012, 185–186, 100–107. DOI: 10.1016/j.cej.2012.01.050.

[5] WANG H.Q., YANG G.F., LI Q.Y., ZHONG X.X., WANG F.P., LI Z.S., LI Y.H., *Porous nanoMnO2: large scale synthesis via a facile quick-redox procedure and application in a supercapacitor*, New J. Chem., 2011, 35, 469–475. DOI: 10.1039/C0NJ00712A.

[6] MARSHALL V.M., LEWIS M.M., OSTENDORF B., *Buffelgrass (Cenchrus ciliaris) as an invader and threat to biodiversity in arid environments. A review*, J. Arid. Environ., 2012, 78, 1–12. DOI: 10.1016 /j.jaridenv.2011.11.005.

[7] WANG S.G., GONG W.X., LIU X.W., YAO Y.W., GAO B.Y., YUE Q.Y., *Removal of lead(II) from aqueous solution by adsorption onto manganese oxide-coated carbon nanotubes*, Sep. Purif. Technol., 2007, 58, 17–23. DOI: 10.1016/j.seppur.2007.07.006.

[8] ZOU W., HAN R., CHEN Z., SHI J., HONGMIN L., *Characterization and properties of manganese oxide coated zeolite as adsorbent for removal of copper(II) and lead(II) ions from solution*, J. Chem. Eng., 2006, 51, 534–541. DOI: 10.1021/je0504008.

[9] DEMIRKIRAN N., *Copper adsorption by natural manganese dioxide*, T. Nonfer. Metal. Soc., 2015, 25, 647–653. DOI: 10.1016/S1003-6326 (15)63648-2.

[10] WANG S., GAO B., LI Y., MOSA A., ZIMMERMAN A.R., MA L.Q., HARRIS W.G., MIGLIACCIO K.W., *Manganese oxide-modified biochars: preparation, characterization, and sorption of arsenate and lead*, Biores. Technol., 2015, 181, 13–17. DOI: 10.1016/j.biortech.2015.01.044.

[11] MALIYEKKAL S.M, SHARMA A.K., PHILIP L., *Manganese-oxide-coated alumina. A promising sorbent for defluoridation of water*, Water Res., 2006, 40, 3497. DOI: 10.1016/j.watres.2006.08.007.

[12] WU K., LIU T., XUE W., WANG X., *Arsenic(III) oxidation/adsorption behaviors on a new bimetal adsorbent of Mn-oxide-doped Al oxide*, Chem. Eng. J., 2012, 192, 343–349. DOI: 10.1021/es061160z.

[13] JAFTA C.J., NKOSI F., ROUX L.L., MATHE M.K., KEBEDE M., MAKGOPA K., SONG Y., TONG D., OYAMA M., MANYALA N., CHEN S., OZOEMENA K.I., *Manganese oxide/graphene oxide composites for high-energy aqueous asymmetric electrochemical capacitors*, Electrochim. Acta, 2013, 110, 228–233. DOI: 10.1016/j.electacta.2013.06.096.

[14] SUN K., WANG H., PENG H., WU Y., MA G., LEI Z., *Manganese oxide nanorods supported on orange peel-based carbon nanosheets for high performance supercapacitors*, Int. J. Elect. Sci., 2015, 10, 2000–2013.

[15] WANG L., HU C., SHAO L., *Antimicrobial activity of nanoparticles: present situation and prospects for the future*, Int. J. Nanomed., 2017, 12, 1227–1249. DOI: 10.2147/IJN.S121956.

[16] LAGERGREN S., *About the theory of so called adsorption of soluble substances*, Kungliga Svenska Vetenskapsakademiens Handlingar, 1898, 24 (4), 1–39.

[17] HO Y.S., MCKAY G., *Pseudo-second order model for sorption processes*, Proc. Biochem., 1999, 34, 451–465. DOI: 10.1016/S0032-9592 (98)00112-5.

[18] TRAN M.V., HA A.T., LE P.M.L., *Nanoflake manganese oxide and nickel-manganese oxide synthesized by electrodeposition for electrochemical capacitor*, J. Nanomater., 2015, Article ID 609273, 1–13. DOI: 10.1021/ac5039863.

[19] MALAR C.G., SEENUVASAN M., SATHISHKUMAR K., *Adsorption of nickel ions by surface modified magnetite nanoparticles: kinetic study*, J. Environ. Biol., 2019, 40, 748–752. DOI: 10.22438/jeb/40/4 (SI)/JEB_10.

[20] LENOBLE V., LACLAUTRE C., SERPAUD B., DELUCHAT V., BOLLINGER J.C., *As(V) retention and As(III) simultaneous oxidation and removal on a MnO2-loaded polystyrene resin*, Sci. Total. Environ., 2004, 326, 197–207. DOI: 10.1016/j.scitotenv.2003.12.012F.

[21] PANNEERSELVAM P., MORAD N., TAN A.K., *Magnetic nanoparticle (Fe3O4) impregnated onto tea waste for the removal of nickel(II) from aqueous solution*, J. Hazard. Mater., 2011, 186, 160–168. DOI: 10.1016/j.jhazmat.2010.10.102.

[22] HALDER G., KHAN A.A., DHAWANE S., *Fluoride sorption onto a steam-activated biochar derived from cocos nucifera shell*, Clean-Soil Air Water, 2016, 44 (2), 124–133. DOI:10.1002/clen.201400649.

[23] MAHAPATRA A., MISHRA B.G., HOTA G., *Electrospun Fe2O3–Al2O3 nanocomposite fibers as efficient adsorbent for removal of heavy metal ions from aqueous solution*, J. Hazard. Mater., 2013, 258–259, 116–123. DOI: 10.1016/j.jhazmat.2013.04.045.

[24] SPARKS D.L., SUAREZ D.L. (Eds.), *Rate of Soil Chemical Processes*. SSSA Spec. Publ. 27, SSSA, Madison, WI, 1991.

[25] SHIKUKU V.O., ZANELLA R., KOWENJE C.O., DONATO F.F., BANDEIRA N.M.G., PRESTES O.D., *Single and binary adsorption of sulfonamide antibiotics onto iron-modifed clay: linear and nonlinear isotherms, kinetics, thermodynamics, and mechanistic studies*, Appl. Water Sci., 2018, 8, 175. DOI: 10.1007/s13201-018-0825-4.

[26] YU Y., ZHUANG Y.Y., WANG Z.H., *Adsorption of water-soluble dye onto functionalized resin*, J. Coll. Interf. Sci., 2001, 242, 288–293. DOI: 10.1006/jcis.2001.7780.